Active and Passive Beamforming Optimization For Distributed STAR-RIS-Assisted Multi-User MISO Systems

Ha An Le, Trinh Van Chien, *Member*, *IEEE*, and Wan Choi, *Fellow*, *IEEE*

***Abstract*—This paper investigates a joint active and passive beamforming design for distributed simultaneous transmitting and reflecting (STAR) reconfigurable intelligent surface (RIS) assisted multi-user (MU)- mutiple input single output (MISO) systems, where the energy splitting (ES) mode is considered for the STAR-RIS. We aim to design the active beamforming vectors at the base station (BS) and the STAR-RIS scattering coefficients to maximize the user sum rate under transmitting power constraints. The formulated problem is non-convex and nontrivial to obtain the global optimum due to the coupling between active beamforming vectors and STAR-RIS phase shifts. To efficiently solve the problem, we propose two novel approaches, namely alternating optimization (AO)-based and graph neural network (GNN)-based frameworks. Specifically, the former splits the original problem into active beamforming, STAR-RIS phase shifts, and STAR-RIS amplitude coefficients sub-problems and solve them in an iterative manner. Furthermore, successive convex approximation (SCA) method is applied to obtain the solution for each sub-problem satisfying Karush-Kuhn-Tucker (KKT) conditions. The latter exploits a heterogeneous GNN to capture the interactions among users and network entities, and directly optimizes beamforming vectors and STAR-RIS coefficients with the system objective. Numerical results show that both proposed approaches yield efficient performance compared to the previous benchmarks. Furthermore, the proposed GNN is scalable with various system configurations.**

***Index Terms*—Reconfigurable intelligent surface, graph neural network, deep learning, beamforming.**

I. Introduction

Beyond fifth-generation (B5G) and sixth-generation (6G) wireless communication networks are expected to cope with the explosive increase in the number of wireless devices with a focus on spectral and energy efficiency [1]. In this light, RISs have emerged as a promising technology capable of significantly enhancing the sum rate and energy efficiency of wireless networks. [2]. An RIS is a flat meta-surface containing a number of inexpensive passive reflecting components, which can be adjusted through a controller linked to the BS to smartly manage the propagation of the incident signals with low power consumption. Moreover, RIS deployment allows for the establishment of a virtual connection between the BS and user equipment (UE), especially in scenarios where they are situated in areas with no service or where direct links are obstructed. Nevertheless, conventional RISs are only capable of reflecting incident signals, hence only users located in the 180^o half-plane can be supported by the RISs. Consequently, the positioning of both the BS and users is constrained to be on the same side as the RISs, which restricts their deployment possibilities. As a remedy, the STAR-RIS emerges as a promising technology that overcomes the constraints of conventional RIS setups as it can extend the coverage from half-space to a complete 360^o space [3]. Specifically, the STAR-RIS divides the three-dimensional (3D) space into two distinct regions, i.e., the transmission region (T region) and the reflection region (R region). Therefore, compared to conventional RISs, STAR-RISs can introduce new degrees-of-freedom (DoFs) that enhance the system performance [3].

Due to its significant potential, researchers in both industry and academia have directed considerable attention toward STAR-RIS and its variations. Many works have exploited the STAR-RISs technology in various system settings. In [3], the authors examined a MISO system aided by STAR-RIS, and focused on a problem aimed at minimizing power consumption while considering active and passive beamforming. Furthermore, STAR-RISs are employed in non-orthogonal multiple access (NOMA) systems to enhance the performance gain. In [4], the authors delve into a problem of optimizing both active beamforming vectors and STAR-RIS phase shifts to enhance the energy efficiency and overall sum rate of NOMA systems. An iterative-base semidefinite relaxation (SDR) scheme is proposed to tackle the non-convexity. In [5], the authors examined the coverage characterization of a two-user system aided by STAR-RIS with a joint optimization of power allocation at the access point and the STAR-RIS scattering coefficients. The non-convex decoding order constraint in the problem is re-transformed into a convex one by applying KKT conditions. Nevertheless, most of the current research has focused on single STAR-RIS-assisted wireless systems. The benefits of deploying multiple intelligent reflecting surfaces have been investigated in [6]–[8]. Compared to the single RIS case, the distributed employment can improve the coverage, signal power, and system energy efficiency. Hence, it is crucial to study a distributed STAR-RIS-assisted systems.

While STAR-RISs have been extensively explored in the existing literature, traditional designs face challenges due to their high computational complexity. Unlike conventional RIS systems, both amplitude coefficients and phase shifts should be jointly designed in STAR-RIS systems, which further increases the system's complexity. In this light, deep learning (DL) has stood out as a cost-effective solution for the system optimization [9]–[14]. Particularly, fully connected neural networks (FCNNs) were proposed in [9] to approximate an iterative process in resource management. FCNNs were trained via a supervised training procedure with known labels to obtain a local optimum solution of the WMMSE solution. Furthermore, convolutional neural networks (CNNs) were pro-

Ha An Le and Wan Choi are with the Department of Electrical and Computer Engineering, Seoul National University, Seoul, Korea

Trinh Van Chien is with the School of Information and Communications Technology (SoICT), Hanoi University of Science and Technology, Hanoi 100000, Vietnam.

posed to predict optimal beamforming vectors from channel information in [10], [11]. Convolutional layers are utilized to extract spatial channel correlation information and estimate the optimal beamforming vectors. Regarding the RIS designs, the authors in [12] applied a deep quantization neural network to perform joint optimization of the active beamforming vectors at the BS and the phase shifts of the RIS, accounting for imperfect CSI. In addition, an end-to-end design for a double-RIS aided MIMO system was proposed in [13] to optimize the system's reliability, where each device is model as a one-dimensional CNN (1D-CNN) model and are jointly trained to reduce the detected symbol error rate. DL models have also found application in optimizing STAR-RIS systems. In [14], a DRL model was introduced to collectively predict both the active beamforming and STAR-RIS phase shift elements, aiming to improve energy efficiency. Despite the remarkable performance and low complexity of conventional DL models, they lack generalizability to different network sizes, such as different numbers of users and RIS elements. Due to the model's fixed output/input dimension nature, an FCNN/CNN trained with a particular configuration is not able to be applied to other configurations. This issue greatly limits the applicability of DL models in practice, where the system configuration changes dynamically over time. One possible solution for this problem is to train multiple DL models with different configurations and switch them respectively with the real system setting. This is indeed a cook-up solution since prohibitively high training complexity and storage memory are required.

Considering the dimensional limitations of conventional FCNN/CNN models, the key goal is to find a DL design for distributed STAR-RIS-aided MU-MISO systems that are scalable to different system settings with varying numbers of users and STAR-RIS elements. To achieve this, the designed deep neural network (DNN) should be dimensional-invariant to the input regardless of system configurations. The evolution of these neural networks has been explored within the framework of (GNNs) [15], which were originally designed to manage graph-structured data. Each GNN layer is carefully designed to be invariant to different input dimensions and order, thus preserving the permutation invariant (PI) and permutation equivariance (PE) of the model [16]. In other words, GNNs are able to learn the underline interaction between network entities and generalize well with the varying number of order of them. Motivated by this property, GNNs have been extended to solve many scalable wireless communication systems [17]–[22]. In [17]–[19], the homogeneous GNN was utilized to address power management concerns within device-to-device (D2D) wireless networks, where each transmitter-receiver pair is model as a vertex of the graph, and their interfering channels are model as edges. Due to the sharing of trainable parameters between vertices, these GNN models achieve a remarkable generalizing performance among different numbers of transceiver pairs. Moreover, GNN models are applied to more complex wireless networks where devices belong to different types of vertices. In [20], [21], heterogeneous GNN was applied to model MU-MISO systems. This approach involved representing each antenna and user as distinct types of vertices, and the explicit channels between them are exploited as weights of edges in the graph. By exchanging information between two types of vertices through a heterogeneous message passing inference, the designed GNN models are able to estimate the precoding matrix and achieve a remarkable performance compared to the conventional beamforming solutions.

A. Contributions

Motivated by the above challenges and the recent success of GNN, this paper investigates the optimization problem of jointly optimizing active and passive beamforming for distributed STAR-RIS-aided MU-MISO systems. In particular, we study the simultaneous designs of the active beamforming vectors at the BS, the STAR-RIS phase shifts, and the STAR-RIS amplitude coefficients to maximize the sum rate of users while operating within specified power constraints. With the considered problem, we propose two different approaches namely alternating optimization (AO)-based, and heterogeneous graph neural network (HGNN)-based approach. For the AO-based approach, we use an alternating optimization method to handle the coupling variables. Moreover, the non-convexity of each sub-problem is overcome by successive convex approximation (SCA) method. For the second approach, we propose an HGNN design where each element of the STAR-RIS and each user are represented as distinct types of vertices within the graph structure. The information between them is then propagated through the entire graph via a heterogeneous message-passing procedure dedicated to the considered problem. The designed HGNN is then trained via an unsupervised fashion to enhance the system sum rate. Our primary contributions are outlined as follows

- We formulate a sum rate optimization problem for distributed STAR-RIS-assisted MU-MISO systems. To address the non-convex nature of the problem, we partition the original problem into three sub-problems corresponding to each optimization variable, i.e. active beamforming vectors, STAR-RIS phase shifts, and STAR-RIS amplitude coefficients, then solve them with an AO-based algorithm. Furthermore, we apply the SCA to approximate the non-convex sub-problem, transforming it into a convex form. The problem is then optimized by an iterative manner.
- We investigate the PE property of the beamforming policy in the considered system and propose a heterogeneous graph representation to model the considered wireless networks. Each STAR-RIS element and user is modeled as a vertex of the graph, and the corresponding equivalent channel is used as edges connecting them. Consequently, we propose a heterogeneous graph message passing (HGMP) algorithm dedicated to beamforming tasks which facilitates the information exchange through the entire graph. We then prove that the PE property is well-preserved in the proposed HGMP.
- We present an effective implementation of the beamforming heterogeneous graph neural network (BHGNN) model executing the proposed message-passing algorithm. Specifically, each of the functions in the HGMP

algorithm is approximated by an FCNN model with trainable parameters. The forward propagation of the designed BHGNN model is executed aligned with the HGMP algorithm and the model is then trained to optimize the system sum rate. Since the vertices and edges dimension is invariant to the system configuration the designed BHGNN can generalize well with different system settings, making it practical to dynamic networks.

- We produce extensive simulations to validate the efficacy of the proposed methodologies. The numerical results indicate that the HGNN can attain performance levels close to those of the AO-based approach with much lower computational complexity. Moreover, the HGNN model generalizes well with various numbers of users, STAR-RIS elements, and user distributions.

The rest of this paper is organized as follows: Section II introduces the system model and outlines the formulation of the problem aiming to maximize user sum rates. In section III an AO-based solution is presented to address the formulated problem. Section IV introduces a heterogeneous graph representation for the system and proposes a GNN-based solution to jointly optimize beamforming vectors and STAR-RIS phase shifts, maximizing the system sum rate. The numerical results and discussions are detailed in Section V, and Section VI offers the primary conclusions drawn from this paper.

Notation: Matrices are presented by bold capital letters, and lower bold letters denote vectors. The regular transpose and Hermitian transpose of a matrix $\mathbf{A}$ are denoted by $\mathbf{A}^T$ and $\mathbf{A}^H$, respectively. The trace of a square matrix $\mathbf{A}$ is denoted by $\mathrm{tr}(\mathbf{A})$, while its inverse is represented as $\mathbf{A}^{-1}$. Furthermore, $\mathcal{R}(.)$ and $\mathcal{I}(.)$ are employed to represent the real and imaginary parts, respectively, of the given argument. $\|\cdot\|$ represents the Euclidean norm, and $\mathcal{CN}(\cdot,\cdot)$ is a circularly symmetric Gaussian distribution. $\nabla f(\cdot)$ denotes the derivative of function $f(\cdot)$. Finally, $\mathcal{O}(\cdot)$ is the big-$\mathcal{O}$ notation.

II. System Model and Problem Formulation

This section describe the distributed STAR-RIS system under study in the paper. We formulate a problem aimed at maximizing the sum rate while adhering to constrained power limits, specifically addressing the joint design of active and passive beamforming.

A. System model

We investigate a distributed MISO system aided by STAR-RIS, where a BS with N_t antennas serves K individual users, each equipped with a single antenna, positioned on either the transmission side (t) or the reflection side (r). To enhance the system spectral efficiency, L STAR-RISs are deployed to support the transmission, each of which contains M scattering coefficients. In this paper, we make the assumption that the STAR-RISs function under the energy splitting (ES) mode, which involves dividing the power of the incoming signal into transmitted and reflected signal energies. Consequently, the matrices representing the transmission and reflection coefficients of the l-th STAR-RIS are expressed as

$$\mathbf{\Phi}_l^{\chi} = \mathrm{diag}\left(\sqrt{\beta_{l1}^{\chi}}e^{\theta_{l1}^{\chi}}, \cdots, \sqrt{\beta_{lM}^{\chi}}e^{\theta_{lM}^{\chi}}\right), \tag{1}$$

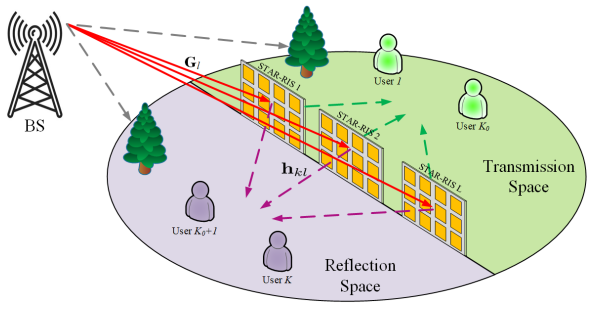

Fig. 1. The considered distributed STAR-RIS system model.

where $\chi \in \{t, r\}$. For compact forms, let us denote $\boldsymbol{\beta}_l^{\chi} = [\sqrt{\beta_{l1}^{\chi}}, \cdots, \sqrt{\beta_{lM}^{\chi}}]^T$, and $\mathbf{\Theta}_l^{\chi} = [e^{j\theta_{l1}^{\chi}}, \cdots, e^{j\theta_{lM}^{\chi}}]^T$ the amplitude and phase shift vectors of the l-th STAR-RIS in the t and r region, respectively. Moreover, in this paper, direct links between the BS and users are assumed to be obstructed by obstacles. Among the K users, we consider the initial K_0 users positioned in the t region, while the rest $(K - K_0)$ users are situated in the r region. Specifically, $\chi = t$ if $k \in 1, 2, \cdots, K_0$, otherwise $\chi = r$. The received signal at the k-th user can be expressed as

$$y_k = \sum_{l=1}^{L} \mathbf{h}_{kl}^H \mathrm{diag}(\boldsymbol{\beta}_l^{\chi}) \mathrm{diag}(\mathbf{\Theta}_l^{\chi}) \mathbf{G}_l \mathbf{x} + n_k, \tag{2}$$

where $\mathbf{x} = \sum_{k=1}^{K} \mathbf{w}_k s_k$ contains the transmitted symbols, and $n_k \sim \mathcal{CN}(0, \sigma^2)$ denotes additive white Gaussian noise. Moreover, $\mathbf{h}_{kl} \in \mathbb{C}^M$ represents the channel from the l-th RIS to the k-th user, and $\mathbf{G}_l \in \mathbb{C}^{M \times N_t}$ signifies the channel from the BS to the l-th RIS. The signal-to-interference-and-noise ratio (SINR) at the k-th user is represented as

$$\gamma_k = \frac{\left|\sum_{l=1}^{L} \mathbf{h}_{kl}^H \mathbf{\Phi}_l^{\chi} \mathbf{G}_l \mathbf{w}_k\right|^2}{\sum_{j \in \mathcal{K}, j \neq k} \left|\sum_{l=1}^{L} \mathbf{h}_{kl}^H \mathbf{\Phi}_l^{\chi} \mathbf{G}_l \mathbf{w}_j\right|^2 + \sigma^2}, \tag{3}$$

where $\mathcal{K} = \{1, 2, \cdots, K\}$ is the set of user. The SINR expression in (3) reveals that compared to a centralized STAR-RIS system, the distributed RISs gain the potential for increased spatial diversity, enhanced interference mitigation by cooperatively optimizing STAR-RIS phase shifts over multiple channel realizations. Moreover, the potential gain is in the order of $\mathcal{O}(L^2M^2)$ thanks to the coherent signal processing.

B. Problem Formulation

Our objective is to maximize the system sum rate of all users while adhering to the transmit power constraint by jointly optimizing the precoding vector $\mathbf{w}_k$, the STAR-RIS phase shift $\mathbf{\Theta}^{\chi}$, and the amplitude coefficients $\boldsymbol{\beta}_l^{\chi}$. Mathematically, the optimization problem is formulated as

$$\underset{\{\mathbf{W}, \mathbf{\Theta}^{\chi}, \boldsymbol{\beta}^{\chi}\}}{\text{maximize}} \quad \sum_{k \in \mathcal{K}} \log_2(1 + \gamma_k) \tag{4a}$$

$$\text{subject to} \quad \mathbf{W}^H \mathbf{W} \leq P_{\max}, \tag{4b}$$

$$\theta_{lm}^{\chi} \in [0, 2\pi], \quad \forall l \in \mathcal{L}, m \in \mathcal{M}, \tag{4c}$$

$$0 \leq \beta_{lm}^{\chi} \leq 1 \quad \forall l \in \mathcal{L}, m \in \mathcal{M}, \tag{4d}$$

$$(\beta_{lm}^T)^2 + (\beta_{lm}^R)^2 \leq 1, \forall l \in \mathcal{L}, m \in \mathcal{M}, \quad (4e)$$

where $\mathcal{M} = \{1, 2, \cdots, M\}$ is the set of STAR-RIS phase shift elements. Besides, $\mathcal{L} = \{1, 2, \cdots, L\}$ is the set of STAR-RISs. The stacked beamforming vector of all K user is $\mathbf{W} = [\mathbf{w}_1^T, \mathbf{w}_2^T, \cdots, \mathbf{w}_K^T]^T \in \mathbb{C}^{N_t K}$. Similarly, the stacked phase shift matrix of all the L STAR-RISs are $\mathbf{\Theta}^\chi = [(\mathbf{\Theta}_1^\chi)^T, \cdots (\mathbf{\Theta}_L^\chi)^T]^T$, $\boldsymbol{\beta}^\chi = [(\boldsymbol{\beta}_1^\chi)^T, \cdots, (\boldsymbol{\beta}_L^\chi)^T]^T$. In (4), $P_{\max}$ is the transmit power budget at the BS, (4b) represents the total transmit power constraint, and (4c) defines the phase shift constraint for each STAR-RIS element. In addition, (4d) and (4e) denote the constraints on the conservation law of energy at the STAR-RIS. One can prove that problem (4) is non-convex and NP-hard by exploiting the same methodology as in [23] with the maximal independent set. Apart from this, the coupling of transmit beamforming and STAR-RIS phase shifts makes problem (4) generally challenging to obtain the global solution. Consequently, in the next sections, we propose two alternative frameworks that obtain feasible solutions for the considered problem, namely an AO-based iterative algorithm and a heterogeneous GNN-based solution.

III. AO-based Solution of Joint Beamforming Optimization Problem

This section proposes an AO-based solution to effectively optimize beamforming vectors and scattering coefficients. Specifically, we decompose problem (4) into three subproblems corresponding to separate variables, i.e. $\mathbf{w}_k$, $\boldsymbol{\beta}^\chi$, and $\mathbf{\Theta}^\chi$, and solve each of them in an iterative manner.

A. Phase shift optimization

For given $\mathbf{w}_k$ and $\boldsymbol{\beta}^\chi$, problem (4) can be re-written as

$$\begin{aligned}
\underset{\mathbf{\Theta}^\chi, \boldsymbol{\eta}}{\text{maximize}} \quad & \sum_{k \in \mathcal{K}} \log_2(1 + \eta_k) && (5a)\\
\text{subject to} \quad & \eta_k \leq \frac{\left|\sum_{l=1}^L \mathbf{h}_{kl}^H \mathbf{\Phi}_l^\chi \mathbf{G}_l \mathbf{w}_k\right|^2}{\sum_{i \in \mathcal{K}, i \neq k} \left|\sum_{l=1}^L \mathbf{h}_{kl}^H \mathbf{\Phi}_l^\chi \mathbf{G}_l \mathbf{w}_i\right|^2 + \sigma^2} \\
& \forall k \in \mathcal{K}, && (5b)\\
& \theta_{lm}^k \in [0, 2\pi], \quad \forall l \in \mathcal{L}, m \in \mathcal{M}, && (5c)
\end{aligned}$$

where $\boldsymbol{\eta} = [\eta_1, \cdots, \eta_k]^T$ stands as a slack variable, ensuring the constraint (5b) remains satisfied at all times, maintaining equality at the optimal solution. Let us denote $s_{ln}^\chi = e^{j\theta_{ln}^\chi}$, then we can show that $\mathbf{h}_{kl}^H \text{diag}(\boldsymbol{\beta}_l^\chi) \mathbf{\Theta}_l^\chi \mathbf{G}_l \mathbf{w}_i = \mathbf{t}_{kil}^H \mathbf{s}_l^\chi$, where $\mathbf{t}_{kil} = (\text{diag}(\mathbf{h}_{kl}^H) \text{diag}(\boldsymbol{\beta}_l^\chi) \mathbf{G}_l \mathbf{w}_i)^* \in \mathbb{C}^M$, and $\mathbf{s}_l^\chi = [s_{l1}^\chi, \cdots, s_{lM}^\chi]$. The constraint (5b) can be reformulated as

$$\eta_k \leq \frac{|\mathbf{t}_{kk}^H \mathbf{s}^\chi|^2}{\sum_{i \in \mathcal{K}, i \neq k} |\mathbf{t}_{ki}^H \mathbf{s}^\chi|^2 + \sigma^2}, \quad (6)$$

where the new vectors are defined as $\mathbf{s}^\chi = [s_{11}^\chi, \cdots, s_{1M}^\chi, \cdots, s_{LM}^\chi]^T$, and $\mathbf{t}_{ki} = [\mathbf{t}_{ki1}; \cdots; \mathbf{t}_{kiL}]$. Consequently, problem (5) can be reformulated as

$$\begin{aligned}
\underset{\mathbf{w}}{\text{maximize}} \quad & \sum_{k \in \mathcal{K}} \log_2(1 + \eta_k) && (7a)\\
\text{subject to} \quad & |s_{lm}^\chi| = 1, \quad \forall l \in \mathcal{L}, m \in \mathcal{M}, && (7b)\\
& \eta_k \leq \frac{|\mathbf{t}_{kk}^H \mathbf{s}^\chi|^2}{\sum_{i \in \mathcal{K}, i \neq k} |\mathbf{t}_{ki}^H \mathbf{s}^\chi|^2 + \sigma^2}, \forall k \in \mathcal{K}. && (7c)
\end{aligned}$$

Problem (7) is, however, still non-convex owing to the presence of the unit modulo constraint and the non-convex nature of constraints (6). We first relax the unit modulo constraint by applying the penalty method and the objective function now can be expressed as

$$\sum_{k=1}^K \log_2(1 + \eta_k) + C \sum_{k=1}^K \sum_{l=1}^L \sum_{m=1}^M (|s_{lm}^\chi|^2 - 1), \quad (8)$$

with C is a large positive constant. Next, the SCA method is applied to handle the non-convex objective and constraints. We first provide an useful proposition on the first order Taylor approximation of a complex function.

Proposition 1. *Let us consider $f(\mathbf{x}) \triangleq |\mathbf{a}^H \mathbf{x} + b|^2$, where $\mathbf{a}, \mathbf{x}$, and b are complex vectors with compatible dimensions. The first order Taylor approximation of $f(\mathbf{x})$ at the n-th iteration is given as*

$$f(\mathbf{x}) \approx |\mathbf{a}^H \mathbf{x}^{(n)} + b|^2 + 2\mathcal{R}((\mathbf{a}^H \mathbf{x}^{(n)} + b)^H \mathbf{a}^H (\mathbf{x} - \mathbf{x}^{(n)})), \quad (9)$$

where $\mathbf{x}^{(n)}$ is the solution of $\mathbf{x}$ at the n-th iteration from an initial $\mathbf{x}^{(0)}$.

Proof: The first order Taylor approximation of $f(\mathbf{x})$ at the n-th iteration follows the Taylor's formula as

$$f(\mathbf{x}) \approx f(\mathbf{x}^{(n)}) + df(\mathbf{x}^{(n)})(\mathbf{x} - \mathbf{x}^{(n)}). \quad (10)$$

The first term in (9) is obtained by plugging $\mathbf{x}^{(n)}$ into $f(\mathbf{x})$. We now calculate the second term. The derivative of $f(\mathbf{x})$ is calculated following Leibniz's rule as

$$\begin{aligned}
\frac{df(\mathbf{x})}{d\mathbf{x}} &= \frac{d(\langle \mathbf{a}^H \mathbf{x} + b, \mathbf{a}^H \mathbf{x} + b \rangle)}{d\mathbf{x}} \\
&= \langle \frac{d(\mathbf{a}^H \mathbf{x} + b)}{d\mathbf{x}}, \mathbf{a}^H \mathbf{x} + b \rangle + \langle \mathbf{a}^H \mathbf{x} + b, \frac{d(\mathbf{a}^H \mathbf{x} + b)}{d\mathbf{x}} \rangle \\
&= \langle \mathbf{a}^H, \mathbf{a}^H \mathbf{x} + b \rangle + \langle \mathbf{a}^H \mathbf{x} + b, \mathbf{a}^H \rangle,
\end{aligned} \quad (11)$$

where $\langle \cdot, \cdot \rangle$ is the inner product of two vectors. Thus, the second term in (9) can be computed as

$$\begin{aligned}
&df(\mathbf{x}^{(n)})(\mathbf{x} - \mathbf{x}^{(n)}) \\
&= \langle \mathbf{a}^H (\mathbf{x} - \mathbf{x}^{(n)}), \mathbf{a}^H \mathbf{x}^{(n)} + b \rangle + \langle \mathbf{a}^H \mathbf{x}^{(n)} + b, \mathbf{a}^H (\mathbf{x} - \mathbf{x}^{(n)}) \rangle \\
&= 2\mathcal{R}((\mathbf{a}^H \mathbf{x}^{(n)} + b)^H \mathbf{a}^H (\mathbf{x} - \mathbf{x}^{(n)}),
\end{aligned} \quad (12)$$

Plugging (11) and (12) into (10), we complete the proof. ■

Applying Proposition 1 allows us to approximate (8) as

$$\begin{aligned}
&\sum_{k=1}^K \log_2(1 + \eta_k) + \\
&2C \sum_{k=1}^K \sum_{l=1}^L \sum_{m=1}^M \mathcal{R}(((s_{lm}^\chi)^{(n)})^H (s_{lm}^\chi - (s_{lm}^\chi)^{(n)})))
\end{aligned} \quad (13)$$

To handle the non-convexity in the constraints (6), we introduce a slack variable α_k and decompose each constraint of (6) into two following constraints

$$|\mathbf{t}_{kk}^H \mathbf{s}^\chi|^2 \geq \alpha_k \eta_k, \quad (14)$$

Algorithm 1 SCA for solving problem (5)

1: Initialization: $(\mathbf{s}^{\chi})^{(0)}, \alpha_k^{(0)}, \eta_k^{(0)}, k \in \{1,2\}$ and the iteration index $n=0$.
2: **repeat**
3: Solve the convex problem (17) to obtain $(\hat{\mathbf{s}}^{\chi})^{(n)}, \hat{\alpha}_k^{(n)}, \hat{\eta}_k^{(n)}, k \in \mathcal{K}$.
4: Update $(\mathbf{s}^{\chi})^{(n+1)} = (\mathbf{s}^{\chi})^{(n)} + \gamma((\hat{\mathbf{s}}^{\chi})^{(n)} - (\mathbf{s}^{\chi})^{(n)})$.
5: $\alpha_k^{(n+1)} = \hat{\alpha}_k^{(n)} + \gamma(\hat{\alpha}_k^{(n)} - \alpha_k^{(n)})$
6: $\eta_k^{(n+1)} = \hat{\eta}_k^{(n)} + \gamma(\hat{\eta}_k^{(n)} - \eta_k^{(n)})$
7: $t := t+1$.
8: **until** The fractional increment in the objective function in (17) remains below a specified threshold $\epsilon_1 > 0$.
9: **Return** $\mathbf{s}^{\chi *} = (\hat{\mathbf{s}}^{\chi})^{(n)}, \alpha_k^* = \hat{\alpha}_k^{(n)}, \eta_k^* = \hat{\eta}_k^{(n)}, k \in \mathcal{K}$.

$$\sum_{i \in \mathcal{K}, i \neq k} |\mathbf{t}_{ki}^H \mathbf{s}^{\chi}|^2 + \sigma^2 \leq \alpha_k, \tag{15}$$

where (15) is already convex as aligned with the second-order cone. To address the non-convex nature of (14), we employ the Taylor approximation for both sides as

$$\begin{aligned} &2\mathcal{R}((\mathbf{t}_{kk}^H (\mathbf{s}^{\chi})^{(n)})^H \mathbf{t}_{kk}^H (\mathbf{s}^{\chi} - (\mathbf{s}^{\chi})^{(n)})) + \\ &|\mathbf{t}_{kk}^H (\mathbf{s}^{\chi})^{(n)}|^2 \geq \alpha_k^{(n)} \alpha_k + \eta_k^{(n)} \eta_k - \alpha_k^{(n)} \eta_k^{(n)}. \end{aligned} \tag{16}$$

Overall, problem (5) can be reformulated as the following approximated convex problem

$$\begin{aligned} \underset{\mathbf{s},\eta,\alpha}{\text{maximize}} \quad & \sum_{k \in \mathcal{K}} \log_2(1+\eta_k) + && (17a) \\ & 2C \sum_{k=1}^{K} \sum_{l=1}^{L} \sum_{m=1}^{M} \mathcal{R}(((s_{lm}^{\chi})^{(n)})^H (s_{lm}^{\chi} - (s_{lm}^{\chi})^{(n)}))) \\ \text{subject to} \quad & \alpha_k \geq 0, \quad \forall k \in \mathcal{K}, && (17b) \\ & |s_{lm}^{\chi}| \leq 1, \quad \forall l \in \mathcal{L}, m \in \mathcal{M}, && (17c) \\ & (15), (16), \quad \forall k \in \mathcal{K}. && (17d) \end{aligned}$$

We denote the optimal points of (17) at the n-th SCA iteration as $(\hat{\mathbf{s}}^{\chi})^{(n)}$, $\hat{\alpha}_k^{(n)}$, $\hat{\eta}_k^{(n)}$, the update of variables is given as

$$(\mathbf{s}^{\chi})^{(n+1)} = (\mathbf{s}^{\chi})^{(n)} + \gamma^{(n)}((\hat{\mathbf{s}}^{\chi})^{(n)} - (\mathbf{s}^{\chi})^{(n)}), \tag{18}$$

$$\alpha_k^{(n+1)} = \alpha_k^{(n)} + \gamma^{(n)}(\hat{\alpha}_k^{(n)} - \alpha_k^{(n)}), \tag{19}$$

$$\eta_k^{(n+1)} = \eta_k^{(n)} + \gamma^{(n)}(\hat{\eta}_k^{(n)} - \eta_k^{(n)}), \tag{20}$$

where $\gamma^{(n)}$ is the SCA update step-size chosen following the diminishing rule as $\sum_{n=1}^{\infty} \gamma^{(n)} = +\infty$, and $\sum_{n=1}^{\infty} (\gamma^{(n)})^2 \leq +\infty$. The SCA for solving (5) is summarized in Algorithm 1.

Lemma 1. *If the step-size $\gamma^{(n)}$ satisfies the diminishing step-size rule, the variables $(\mathbf{s}^{\chi})^{(n)}$, $\alpha_k^{(n)}$, $\eta_k^{(n)}$ converge to the points that fulfill the KKT of the original problem* (5).

Proof: Please refer to Appendix A. ∎

Lemma 1 demonstrates that by solving the sequence of approximate problem (17) as in Algorithm 1, we can conduct a series of feasible solutions that eventually converge to the KKT solution of problem (5).

B. Amplitude vector optimization

For given $\boldsymbol{\Theta}$ and $\mathbf{w}_k$, problem (4) can be reduced to as

$$\begin{aligned} \underset{\boldsymbol{\beta}^{\chi},\boldsymbol{\delta}}{\text{maximize}} \quad & \sum_{k \in \mathcal{K}} \log_2(1+\delta_k) && (21a) \\ \text{subject to} \quad & \delta_k \leq \frac{\left|\mathbf{v}_{kk}^H \boldsymbol{\beta}^{\chi}\right|^2}{\sum_{i \in \mathcal{K}, i \neq k} \left|\mathbf{v}_{ki}^H \boldsymbol{\beta}^{\chi}\right|^2 + \sigma^2} \quad \forall k \in \mathcal{K}, && (21b) \\ & (4d), (4e), && (21c) \end{aligned}$$

where $\boldsymbol{\delta} = [\delta_1, \cdots, \delta_K]^T$, $\mathbf{v}_{ki} = [\mathbf{v}_{ki1}; \cdots; \mathbf{v}_{kiL}]$, and $\mathbf{v}_{kil} = (\text{diag}(\mathbf{h}_{kl}^H)\text{diag}(\boldsymbol{\Theta}_l^{\chi})\mathbf{G}_l \mathbf{w}_i)^* \in \mathbb{C}^M$. Applying a methodology akin to that in Section III-A, we can apply the SCA to solve problem (21).

C. Beamforming Optimization

For given $\boldsymbol{\Theta}^{\chi}$ and $\boldsymbol{\beta}^{\chi}$, problem (4) can be reduced to as

$$\begin{aligned} \underset{\mathbf{w},\boldsymbol{\zeta}}{\text{maximize}} \quad & \sum_{k \in \mathcal{K}} \log_2(1+\zeta_k) && (22a) \\ \text{subject to} \quad & \zeta_k \leq \frac{|\tilde{\mathbf{g}}_k^H \mathbf{w}_k|^2}{|\sum_{i \in \mathcal{K}, i \neq k} \tilde{\mathbf{g}}_k^H \mathbf{w}_i|^2 + \sigma^2} \quad \forall k \in \mathcal{K}, && (22b) \\ & \mathbf{W}^H \mathbf{W} <= P_{\max}, && (22c) \end{aligned}$$

where $\boldsymbol{\zeta} = [\zeta_1, \cdots, \zeta_k]^T$ and $\tilde{\mathbf{g}}_k = \sum_{l=1}^{L} \mathbf{G}_l^H \text{diag}(\boldsymbol{\beta}_l^{\chi}) \text{diag}(\boldsymbol{\Theta}_l^{\chi})^H \mathbf{h}_{kl}$. We reframe the constraint (22b) by introducing a slack variable $\gamma_k \geq 0$ as

$$|\tilde{\mathbf{g}}_k^H \mathbf{w}_k|^2 \geq \gamma_k \zeta_k, \tag{23}$$

$$\left| \sum_{i \in \mathcal{K}, i \neq k} \tilde{\mathbf{g}}_k^H \mathbf{w}_i \right|^2 + \sigma^2 \leq \gamma_k. \tag{24}$$

The expression $\tilde{\mathbf{g}}_k^H \mathbf{w}_k$ can be rendered as a real number by applying an arbitrary rotation to $\mathbf{w}_k$. Therefore, constraint (23) is equivalent to $\mathcal{R}(\tilde{\mathbf{g}}_k^H \mathbf{w}_k) \geq \sqrt{\gamma_k \zeta_k}$. Through the first-order Taylor approximation, the constraint (23) can be approximated as

$$\begin{aligned} \mathcal{R}(\tilde{\mathbf{g}}_k^H \mathbf{w}_k) \geq & \sqrt{\gamma_k^{(n)} \zeta_k^{(n)}} + \frac{1}{2} \sqrt{\frac{\gamma_k^{(n)}}{\zeta_k^{(n)}}} (\zeta_k - \zeta_k^{(n)}) \\ & + \frac{1}{2} \sqrt{\frac{\zeta_k^{(n)}}{\gamma_k^{(n)}}} (\gamma_k - \gamma_k^{(n)}). \end{aligned} \tag{25}$$

Then, the non-convex problem (22a) can be reformulated as

$$\begin{aligned} \underset{\mathbf{W},\boldsymbol{\zeta}}{\text{maximize}} \quad & \sum_{k \in \mathcal{K}} \log_2(1+\zeta_k) && (26a) \\ \text{subject to} \quad & \mathbf{W}^H \mathbf{W} \leq P_{\max}, && (26b) \\ & \gamma_k \geq 0, \quad \forall k \in \mathcal{K}, && (26c) \\ & (24), (25), \forall k \in \mathcal{K}. && (26d) \end{aligned}$$

Overall, Algorithm 2 encapsulates the AO-based method tailored for problem (4). The assurance of problem convergence

Algorithm 2 AO-based Algorithm for Solving problem (4)

1: Initialization: $\mathbf{w}^{(0)}, \boldsymbol{\phi}^{(0)}, \boldsymbol{\beta}^{(0)}$, and the iteration index $n = 0$.
2: **repeat**
3: Solve the phase shift optimization problem (5) with given $(\mathbf{w}^{(n-1)}, \boldsymbol{\beta}^{(n-1)})$ utilizing SCA technique in Section III-A, and denote the solution as $\boldsymbol{\phi}^{(n)}$.
4: Solve the amplitude optimization problem (21) with given $(\mathbf{w}^{(n-1)}, \boldsymbol{\phi}^{(n)})$ using SCA technique in Section III-B, and denote the solution as $\boldsymbol{\beta}^{(n)}$.
5: Solve the beamforming optimization problem (26) with given $(\boldsymbol{\phi}^{(n)}, \boldsymbol{\beta}^{(n)})$ using SCA technique in Section III-C, and denote the solution as $\mathbf{w}^{(n)}$.
6: $n := n + 1$.
7: **until** The fractional increment in the objective function in (4a) remains below a specified $\epsilon > 0$.

is underpinned by two fundamental factors. Firstly, as indicated in Lemma 1, the convergence point of the SCA algorithm satisfies the KKT conditions, ensuring that the objective function is non-decreasing through each iteration. Secondly, due to the power constraint and unit-modulo constraint, it is evident that the objective function is upper bound. Therefore, the convergence of Algorithm 2 is guaranteed.

D. Complexity Analysis

The primary complexity of Algorithm 2 arises from tackling the phase shift optimization problem (5), amplitude optimization problem (21), and beamforming optimization problem (26). The complexity associated with solving a problem using SCA is assessed as follows: The required number of inner iterations is $\mathcal{O}(\sqrt{N}\log_2(1/\epsilon_1))$, with N is the number of variables and ϵ_1 is the accuracy of the algorithm. Moreover, the complexity for solving the problem in each inner iteration is $\mathcal{O}(N_1^2 N_2)$, where N_1 is the number of variables and N_2 denotes the number of constraints [24]. Following the analysis, the complexity for solving problem (5) is in order of $\mathcal{O}\left((KLM)^{3.5}\log_2(1/\epsilon_1)\right)$. Similarly, the complexity for solving (21) and (26) are in the order of $\mathcal{O}\left((KLM)^{3.5}\log_2(1/\epsilon_2)\right)$ and $\mathcal{O}\left((N_t K)^{3.5}\log_2(1/\epsilon_3)\right)$, respectively. Consequently, the total complexity of Algorithm 2 is $\mathcal{O}\left(S(KLM)^{3.5}\log_2(1/(\epsilon_1\epsilon_2)) + S(N_t K)^{3.5}\log_2(1/\epsilon_3)\right)$ with S being the number of iterations that Algorithm 2 requires to reach the KKT point.

IV. Graph Neural Network-based Solution

This section introduces a solution based on GNNs to address the considered sum rate optimization problem. We begin by depicting the STAR-RIS multi-user system using a heterogeneous graph. This graph comprises STAR-RIS vertices and user vertices, effectively capturing the dynamic interplay between users and STAR-RISs within the system.

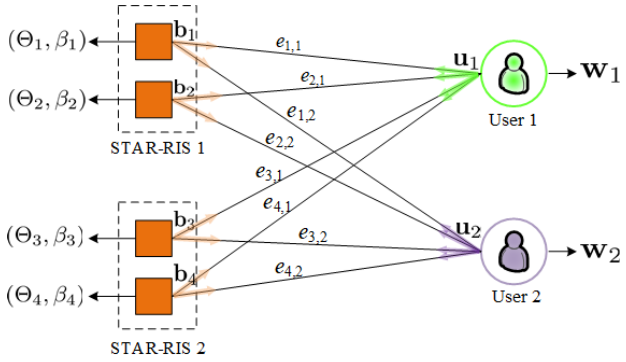

Fig. 2. The graph representation of the distributed STAR-RISs systems.

A. Properties of the joint beamforming design policy

We now show that the optimal active and passive beamforming policy enjoys permutation equivalence properties. We start by re-writing the objective function in (4) as

$$\begin{aligned}\gamma_k &= \frac{|\sum_{l=1}^{L}\sum_{m=1}^{M} h_{klm}\phi_{lm}^{\chi}\mathbf{G}_{lm}\mathbf{w}_k|^2}{\sum_{j\in\mathcal{K},j\neq k}|\sum_{l=1}^{L}\sum_{m=1}^{M} h_{klm}\phi_{lm}^{\chi}\mathbf{G}_{lm}\mathbf{w}_j|^2+\sigma^2} \\ &= \frac{|\sum_{l=1}^{L}\sum_{m=1}^{M} \phi_{lm}^{\chi}\tilde{\mathbf{h}}_{klm}^{H}\mathbf{w}_k|^2}{\sum_{j\in\mathcal{K},j\neq k}|\sum_{l=1}^{L}\sum_{m=1}^{M} \phi_{lm}^{\chi}\tilde{\mathbf{h}}_{klm}^{H}\mathbf{w}_j|^2+\sigma^2},\end{aligned} \tag{27}$$

where $\mathbf{h}_{kl} = [h_{kl1}, \cdots, h_{klM}]^T$, $\mathbf{G}_{lm}$ denotes the m-th row of $\mathbf{G}_l$ and $\tilde{\mathbf{h}}_{klm}^H = h_{klm}\mathbf{G}_{lm} \in \mathbb{C}^{1\times N_t}$ is the equivalent channel between the m-th element of the l-th STAR-RIS and the k-th user including the channel from BS. With the new equivalent objective function, one may view the original system as a system comprising STAR-RIS and users with the corresponding propagation channels between them. We will learn a optimal active and passing beamforming policy as

$$\{\boldsymbol{\Phi}^{\chi*}, \mathbf{W}^*\} = F(\mathbf{H}), \tag{28}$$

where $\mathbf{W}^* = [\mathbf{w}_1^*, \cdots, \mathbf{w}_K^*]$ is the optimal beamforming matrix, $\boldsymbol{\Phi}^{\chi*} = [(\boldsymbol{\Phi}_1^{\chi*})^T, \cdots, (\boldsymbol{\Phi}_L^{\chi*})^T]^T$ denotes the optimal STAR-RIS phase shift, and $\mathbf{H}$ is the equivalent channel matrix between STAR-RIS elements and users, which is expressed as

$$\mathbf{H} = \begin{pmatrix} \tilde{\mathbf{h}}_{111} & \cdots & \tilde{\mathbf{h}}_{K11} \\ \vdots & \vdots & \vdots \\ \tilde{\mathbf{h}}_{11M} & \cdots & \tilde{\mathbf{h}}_{K1M} \\ \vdots & \vdots & \vdots \\ \tilde{\mathbf{h}}_{1LM} & \cdots & \tilde{\mathbf{h}}_{KLM} \end{pmatrix} \in \mathbb{C}^{LM\times K}. \tag{29}$$

Before investigating the PI and PE properties of the joint active and passive beamforming optimization problem, we introduce the definition of these properties. Let consider a multivariate function $\mathbf{Y} = f(\mathbf{X})$, and a permutation matrix $\boldsymbol{\Pi}$, the PI and PE properties of $f(\mathbf{X})$ is defined by the following definition.

Definition 1: For an arbitrary permutation of matrix $\mathbf{X}$*, i.e, denoted by* $\boldsymbol{\Pi}\mathbf{X}$*, if* $\mathbf{Y} = f(\boldsymbol{\Pi}\mathbf{X})$*, then* $\mathbf{Y} = f(\mathbf{X})$ *exhibits permutation invariance to* $\mathbf{X}$*. Additionally, if* $\boldsymbol{\Pi}\mathbf{Y} = f(\boldsymbol{\Pi}\mathbf{X})$*, then* $\mathbf{Y} = f(\mathbf{X})$ *is permutation equivalent to* $\mathbf{X}$*.*

To investigate the properties of the beamforming optimization problem, we first consider a simple example, where there

are 2 STAR-RISs exploited to support the transmission to two users as illustrated in Fig. 2. If the order of two STAR-RISs is swapped, the order of optimal passive beamforming $\mathbf{\Phi}_1^{\chi*}$ and $\mathbf{\Phi}_2^{\chi*}$ is also swapped. In contrast, the beamforming policy defined in (28) remains unchanged. In general, when the order of STAR-RISs is permuted, the optimal STAR-RIS phase shifts, and the rows of $\mathbf{H}$ are permuted to $\mathbf{\Pi}_1\mathbf{\Phi}^{\chi*}$, and $\mathbf{\Pi}_1\mathbf{H}$, respectively. Moreover, when the order of users is permuted, the optimal beamforming vectors and the columns of $\mathbf{\Pi}_1\mathbf{H}$ are permuted to $\mathbf{\Pi}_2\mathbf{W}^*$ and $\mathbf{\Pi}_1\mathbf{H}\mathbf{\Pi}_2^T$. Since the optimal active and passive beamforming optimization policy remains unchanged, we have

$$\mathbf{\Pi}_1\mathbf{\Phi}^{\chi*}, \mathbf{\Pi}_2\mathbf{W}^* = F(\mathbf{\Pi}_1\mathbf{H}\mathbf{\Pi}_2^T). \tag{30}$$

In other words, the optimal beamforming policy is permutation equivariant. By identifying the PE of the beamforming policy, we can design a neural network that not only simply approximates the mapping between channel information and optimal solution, but also preserves this structural property.

B. Heterogeneous Graphical Representation of STAR-RIS systems

We now introduce a comprehensive graphical framework that sheds light on the dynamics of the considered distributed STAR-RIS multi-user system. As illustrated in Fig. 2, the system may be represented as a heterogeneous graph denoted as $\mathcal{G}(\mathcal{V}, \mathcal{E})$, where the STAR-RIS elements and users form two vertex sets denoted as $\mathcal{R}$ and $\mathcal{K}$, where $|\mathcal{R}| = LM$ and $|\mathcal{K}| = K$. In addition, $\mathcal{E}$ comprises the set of undirected edges (i, k) connecting RIS element vertex i and user vertex k, $\forall i \in \mathcal{R}, k \in \mathcal{K}$. To more effectively capture the interaction between user vertices and RIS vertices in the wireless graph, we initially establish the characteristics for each vertex and edge. At a fundamental level, the connection between user k and RIS i can be described by considering the channel information linking them. However, this approach is unsuitable for distributed STAR-RIS systems due to two primary reasons: First, the inherent passive nature of STAR-RIS makes it infeasible to collect instantaneous individual CSI. Second, the absence of a base station within the proposed graphical model suggests that using instant channel information for each edge would inadequately encapsulate the interactions within the wireless system. In this light, it is suggested from the new objective function in the previous subsection that the equivalent channels between STAR-RISs and users is sufficient for the optimization of beamforming and phase shift vectors. To this end, we define the feature for the (r, k) edge connecting the r-th RIS vertex and the k-th user vertex as

$$\mathbf{e}_{r,k} = [\mathcal{R}(\mathbf{H}[r, k]), \mathcal{I}(\mathbf{H}[r, k])], \tag{31}$$

where $\mathbf{H}[r, k]$ denotes the (r, k)-th element of matrix $\mathbf{H}$. The edge feature matrix of the whole graph is then defined as $\mathbf{E} = [\mathbf{e}_{\mathbf{r},\mathbf{k}}] \in \mathbb{R}^{LM\times K\times 2N_t}$. In order to facilitate the exchange of information among vertices, we introduce a graph message passing (GMP) protocol. This protocol enables the dissemination of knowledge across the entire heterogeneous graph, allowing for the collaborative sharing of pertinent statistics required for optimizing the active and passive beamforming vectors. The GMP inference is processed through a series of the T iterations. During each iteration, every vertex communicates with its neighboring vertices, which results in the updating of its internal state by processing the received messages from its adjacent nodes. The update procedure of a vertex state during the t-th iteration can be defined as

- *User vertex update:*

$$\mathbf{u}_k^{(t)} = \mathcal{U}^t(\mathbf{u}_k^{(t-1)}, \mathbf{w}_k^{(t-1)}, \mathbf{c}_k^{(t)}), \tag{32}$$

- *RIS vertex update*

$$\mathbf{b}_r^{(t)} = \mathcal{B}^t(\mathbf{b}_r^{(t-1)}, \Theta_r^{(t-1)}, \beta_r^{(t-1)}, \mathbf{d}_r^{(t)}), \tag{33}$$

where $\mathbf{u}_k^{(t)}$ and $\mathbf{b}_r^{(t)}$ are the vertex feature of the k-th user vertex and r-th RIS vertex at the t-th iteration, respectively. In addition, $\mathcal{U}^t(\cdot)$ and $\mathcal{B}^t(\cdot)$ are user vertex and RIS vertex combination operators. Moreover, $\mathbf{c}_i^t$ and $\mathbf{d}_i^t$ are the aggregated messages from a vertex's neighbors, which are driven as

$$\mathbf{c}_k^{(t)} = \mathrm{PL}_{r\in\mathcal{R}}\{\phi^t(\mathbf{b}_r^{(t-1)}, \mathbf{u}_k^{(t-1)}, \mathbf{e}_{r,k})\}, \tag{34a}$$

$$\mathbf{d}_r^{(t)} = \mathrm{PL}_{k\in\mathcal{K}}\{\psi^t(\mathbf{u}_k^{(t-1)}, \mathbf{b}_r^{(t-1)}, \mathbf{e}_{r,k})\}, \tag{34b}$$

where ϕ^t and ψ^t are the aggregation operators at the user vertices and RIS vertices, and $\mathrm{PL}(.)$ is the pooling function which is dimensional-invariant. In (32) and (33), $\mathbf{w}_k^{(t-1)}$, $\Theta_r^{(t-1)}$, and $\beta_r^{(t-1)}$ are the predicted beamforming vectors, the RIS phase shift and its amplitude at the $(t-1)$-th iteration, which are updated as

$$\mathbf{w}_k^{(t-1)} = \mathcal{W}(\mathbf{u}_k^{(t-1)}), \quad \forall k \in \mathcal{K}, \tag{35a}$$

$$\Theta_r^{(t-1)} = \mathcal{C}(\mathbf{b}_r^{(t-1)}), \quad \forall r \in \mathcal{R}, \tag{35b}$$

$$\beta_r^{(t-1)} = \mathcal{D}(\mathbf{b}_r^{(t-1)}), \quad \forall r \in \mathcal{R}, \tag{35c}$$

where $\mathcal{W}(\cdot)$, $\mathcal{C}(\cdot)$, and $\mathcal{D}(\cdot)$ are the mapping functions. It is worth highlighting that our proposed BMP differs from the conventional message passing procedure, as described in [20] and [25]. In the conventional approach, optimized variables are only predicted at the last iteration, T, of the procedure. Additionally, both types of vertices utilize comparable computation structures for the message generation rule, thereby lacking the capacity to capture the heterogeneous characteristics of the graph network. On the contrary, the proposed BMP predicts beamforming vectors and STAR-RIS phase shifts at each iteration and integrates them into a dedicated message generation rule for each type of vertex. This information will be then propagated throughout the vertices and utilized in subsequent iterations for beamforming and phase shift prediction. We will show in the simulation section that this simple change will enhance the performance of the designed graph neural network. The proposed GMP hinges on the pooling function in (34), enabling the dimension-invariant computation of the graph. We apply the sum operator in the paper, which is a widely recognized and efficient pooling function utilized across various applications [18], [19]. The proposed GMP inference is presented in Algorithm 3.

Algorithm 3 Proposed GMP inference

1: Initialize $\mathbf{u}_k^{(0)}, \mathbf{b}_l^{(0)}, \forall k \in \mathcal{K}, l \in \mathcal{L}$ and $t = 0$.
2: **for** $t \leftarrow 1$ to T **do**
1) *User vertex update:*
The k-th user vertex aggregates its received messages from (34a) to generate message $\mathbf{c}_k^{(t)}$.
The k-th user vertex updates its new feature $\mathbf{u}_k^{(t)}$ from (32) and sends it to the i-th RIS vertex $i \in \mathcal{R}$.
The k-th user generates its corresponding beamforming vector as in (35a).
2) *RIS vertex update:*
The i-th RIS vertex aggregates its received messages from (34b) to generate message $\mathbf{d}_l^{(t)}$.
The i-th RIS vertex updates its new feature $\mathbf{b}_k^{(t)}$ from (33) and sends it to the k-th user vertex $k \in \mathcal{K}$.
The i-th RIS vertex generates its phase shift and amplitude as in (35b) and (35c).
3: **end for**
4: Return the predicted beamforming vectors, RIS phase shift and amplitude at the T-th iteration.

C. Properties of the proposed GMP

This subsection discusses the key properties of the GMP that are favorable to handle the scalable joint beamforming optimization problems.

1) Permutation equivariance: The permutation equivariance property of the GMP is stated in Proposition 2.

Proposition 2. *By denoting the output of the GMP defined in* (32) *and* (33) *as* $\Phi : (\mathbf{E}) \mapsto \mathbf{U}, \mathbf{B}$*, where* $\mathbf{E}$ *is the edge feature tensor,* $\mathbf{U}$ *and* $\mathbf{B}$ *are the output of the GMP corresponding to the user and RIS vertices, i.e., vertex feature at the last layer of GMP,* $\mathbf{\Pi}_1$ *and* $\mathbf{\Pi}_2$ *are RIS and user vertex permutation matrices, we have*

$$\{\mathbf{\Pi}_1\mathbf{B}, \mathbf{\Pi}_2\mathbf{U}\} = \Phi(\mathbf{\Pi}_1\mathbf{E}\mathbf{\Pi}_2^T), \tag{36}$$

for any permutation $\mathbf{\Pi}_1$ *and* $\mathbf{\Pi}_2$.

Proof: Please refer to Appendix A for the detailed proof. ∎

As demonstrated in the previous subsection, the active and passive beamforming policy exhibits a PE property, which signifies that an optimal solution obtained for a permuted problem corresponds to a permutation of the solution derived for the original problem. Proposition 2 states that the GMP respects this property well. Specifically, if a GNN exhibits strong performance on a particular input, its ability to generalize effectively extends to permutations of that input. We emphasize that this property is not naturally guaranteed by FCNNs or CNNs. In contrast, to attain permutation equivariant property, data augmentation is required in the training of FCNNs or CNN with extra computational complexity.

2) Scalability to different system configurations: Due to the dimensional constraints, both FCNNs and CNNs must have the same input and output dimension in the training and testing phases. Therefore, the number of agents in the inference phase can not exceed those in the training phase, which limits the scalability of these networks to various system configurations when the number of UEs varies. In contrast, in the GMP, each vertex with the same type is processed by the same non-linear functions, i.e., $\mathcal{B}(\cdot), \mathbf{U}(\cdot), \phi^t(\cdot)$, and $\psi^t(\cdot)$, whose input dimension is invariant to the number of vertices. Thus, the GMP can be readily adapted to different scales of the considered problem in the testing phase.

D. Implementation of Heterogeneous Graph Neural Network

In this section, we present an implementation of a beamforming heterogeneous graph neural network (BHGNN), which effectively executes the GMP inference described in Algorithm 2. Specifically, we focus on the implementation of the vertex operators, the aggregation operators, and the mapping functions. Instead of finding the exact structure, we adopt various FCNNs to implicitly approximate these functions. The vertex operators and aggregation operators at the t-th layer are designed as

$$\begin{aligned}
\mathbf{u}_k^{(t)} &= f_{\mathcal{U}}^t\big(\mathbf{u}_k^{(t-1)}, \mathbf{w}_k^{(t-1)}, \mathbf{c}_k^{(t)}\big),\\
\mathbf{b}_r^{(t)} &= f_{\mathcal{B}}^t(\mathbf{b}_r^{(t-1)}, \Theta_r^{(t-1)}, \beta_r^{(t-1)}, \mathbf{d}_r^{(t)}),\\
\mathbf{c}_k^{(t)} &= \sum_{r\in\mathcal{R}}(f_\phi^t(\mathbf{b}_r^{(t-1)}, \mathbf{u}_k^{(t-1)}, \mathbf{e}_{r,k})),\\
\mathbf{d}_r^{(t)} &= \sum_{k\in\mathcal{K}}(f_\psi^t(\mathbf{u}_k^{(t-1)}, \mathbf{b}_r^{(t-1)}, \mathbf{e}_{r,k})),\\
\mathbf{w}_k^{(t)} &= f_{\mathcal{W}}(\mathbf{u}_k^{(t)}),\\
\Theta_r^{(t)} &= f_{\mathcal{C}}(\mathbf{b}_r^{(t)}),\\
\beta_r^{(t)} &= f_{\mathcal{D}}(\mathbf{b}_r^{(t)}),
\end{aligned} \tag{37}$$

where $f(\cdot)$ is a FCNN. The reliability of these neural networks is affirmed by the universal approximation theorem [26], affirming that a properly constructed FCNN is able to approximate any continuous function with a sufficiently small error. After the T layers, the beamforming vectors are gathered and normalized to satisfy the transmit power constraint following these steps

$$\begin{aligned}
\mathbf{w}_k^{(T)} &= f_{\mathcal{W}}(\mathbf{u}_k^{(T)}) \in \mathbb{R}^{2N_t},\\
\mathbf{W}^{(T)} &= [\mathbf{w}_1^{(T)}, \cdots, \mathbf{w}_K^{(T)}] \in \mathbb{R}^{2N_t\times K},\\
\mathbf{W}^{(T)} &= \sqrt{P_{\max}}\frac{\mathbf{W}^{(T)}}{||\mathbf{W}^{(T)}||_F},\\
\mathbf{W} &= \mathbf{W}^{(T)}(1:N_t,:) + j\mathbf{W}^{(T)}(N_t+1:2N_t,:),
\end{aligned} \tag{38}$$

where $\mathbf{W}(i_1 : i_2, :)$ denotes a matrix constructed by taking from the i_1-th to i_2-th row of $\mathbf{W}$. Moreover, the STAR-RIS phase shift and amplitude in (2) are obtained as

$$\begin{aligned}
\Theta_r^{(T)} &= f_{\mathcal{C}}(\mathbf{b}_r^{(T)}) \in \mathbb{R}^2, \quad \forall r \in \mathcal{R},\\
\mathbf{\Theta}_l^t &= e^{j2\pi[\Theta_{lM+1}^{(T)}(1),\cdots,\Theta_{(l+1)M}^{(T)}(1)]}, \quad l \in \mathcal{L},\\
\mathbf{\Theta}_l^r &= e^{j2\pi[\Theta_{lM+1}^{(T)}(2),\cdots,\Theta_{(l+1)M}^{(T)}(2)]}, \quad l \in \mathcal{L},\\
\beta_r^{(T)} &= f_{\mathcal{D}}(\mathbf{b}_r^{(T)}) \in \mathbb{R}, \quad \forall r \in \mathcal{R},\\
\boldsymbol{\beta}_l^t &= \left[\sqrt{\beta_{lM+1}^{(T)}}, \cdots, \sqrt{\beta_{(l+1)M}^{(T)}}\right], \quad l \in \mathcal{L},
\end{aligned}$$

$$\boldsymbol{\beta}_l^T = \left[\sqrt{1-\beta_{lM+1}^{(T)}}, \cdots, \sqrt{1-\beta_{(l+1)M}^{(T)}}\right], \quad l \in \mathcal{L}. \quad (39)$$

It is worth noting that in the BHGNN architecture, all vertices utilize the same FCNN structure, which is invariant to the number of UEs as well as STAR-RISs. This is important since it allows the designed BHGNN to be scalable with an arbitrary number of users and STAR-RISs.

E. Training the BHGNN

After obtaining the predicted variables as in (39), the sum rate can be readily computed according to (3) and (4a). In order to train the proposed BHGNN, we define the training minimization problem on the negative expectation of the sum rate as

$$\underset{\boldsymbol{\Omega}}{\text{minimize}} \quad -\mathbb{E}\left[\sum_{k=1}^{K} R_k(\mathbf{W}, \boldsymbol{\Theta}^{\chi}, \boldsymbol{\beta}, \boldsymbol{\Omega})\right], \quad (40)$$

where $\boldsymbol{\Omega} = \{\boldsymbol{\omega}_{\mathcal{D}}, \boldsymbol{\omega}_{\mathcal{D}}, \boldsymbol{\omega}_{\mathcal{C}}, \boldsymbol{\omega}_{\mathcal{U}}, \boldsymbol{\omega}_{\mathcal{B}}, \boldsymbol{\omega}_{\psi}, \boldsymbol{\omega}_{\phi}\}$ is the set of the parameters of the FCNNs. The parameters update can be done using established methods like the mini-batch SGD algorithm, along with its variants such as the Adam algorithm. [27].

F. Complexity Analysis

This section analyzes the computational complexity of the proposed BHGNN model. As described above, BHGNN model comprises multiple FCNN models. For a FCNN model with H hidden layers, its computational complexity is given by [28]

$$C_{\text{FCNN}} = \mathcal{O}\left(Mn_1 + n_H N + \sum_{i=1}^{H-1} n_i n_{i+1}\right), \quad (41)$$

where M, N, and n_i are the input size, the output size, and the number of neural in the i-th layers of the FCNN, respectively. Given the FCNN models designed for the HBGNN in Table I, and by considering the number of vertices of the HBGNN, the total computational complexity of the model is on the order of $\mathcal{O}(LMN_t^2 + KN_t^2 + TN_t)$. Therefore, becomes evident that the proposed HBGNN exibits lower complexity compared to the AO-based SCA algorithm.

V. Numerical Results

This sections evaluates the performance of the distributed STAR-RIS-aided MU-MISO system along with proposed approaches via numerical results. We also compare the distributed and centralized STAR-RIS systems under different aspects.

A. Simulation Settings

We utilize a three-dimensional (3D) Cartesian coordinates to present the positions of devices in the considered system. The BS is situated at the origin, positioned at a height of d_H, where the location of the l-th STAR-RIS is given by $(10 \times l, 0, d_R)$. The users' location is uniformly distributed on the ground in the rectangular area $[20, 30] \times [20, 30]$ in the (x, y)-plane for the T users and $[-30, -20] \times [20, 30]$ in the (x, y)-plane for the R users. If not explicitly stated, we assume the number of antennas to be $N_t = 16$ with the transmit power budget $P_{\max} = 30$ dBm. The number of STAR-RISs is $L = 4$, where the number of scattering coefficients varies according to the scenarios. The channels between the BS and STAR-RISs and between STAR-RISs and users follow the Rician fading channel models as

$$\begin{aligned} \mathbf{G}_l &= \kappa_{1,l}\left(\sqrt{\frac{\xi}{\xi+1}}\bar{\mathbf{G}}_l + \sqrt{\frac{1}{\xi+1}}\tilde{\mathbf{G}}_l\right), \\ \mathbf{h}_{kl} &= \kappa_{2,kl}\left(\sqrt{\frac{\xi}{\xi+1}}\bar{\mathbf{h}}_l + \sqrt{\frac{1}{\xi+1}}\tilde{\mathbf{h}}_l\right), \end{aligned} \quad (42)$$

where $\kappa_{1,l}$ represents the distance path-loss of the channel link modeled as $32.6 + 36.7\log_{10}(d)$, with d signifies the channel link distance measured in meter, $\tilde{\mathbf{G}}_l$ and $\tilde{\mathbf{h}}_l$ denote the non-light-of-sight (NLOS) components, which follow standard Gaussian distributions. In addition, $\bar{\mathbf{G}}_l$ and $\bar{\mathbf{h}}_l$ denote the light-of-sight (LOS) components. We assume the BS antennas are arranged in a ULA structure, while STAR-RISs scattering elements are arranged in the form of a UPA structure. Thus, the LoS components in (42) are expressed as the product of the UPA and ULA response vector [29]. For the AO-based algorithm and the SCA method, we set the penalty factor as $C = 10^4$, the algorithm accuracy as $\epsilon = \epsilon_1 = \epsilon_3 = \epsilon_2 = 10^{-3}$. Moreover, we adopt a three-layer HBGNN model, i.e. $T = 3$, with the deployment of the FCNN presented in Table I. To implement the proposed graph neural network model, we utilize the PyTorch deep learning library [30]. The neural network is trained employing the ADAM optimizer [31], with an initial learning rate of 10^{-3}. Throughout the training phase, the learning rate undergoes reduction every 50 epochs with a decay rate of 0.95. The training process will conclude when the validation loss fails to decrease consistently for five consecutive epochs. To facilitate comparison, we present the performance of the following benchmarks:

1) *AO-SCA*: The iterative algorithm for solving problem (4) presented in Algorithm 2.
2) *BHGNN*: The proposed heterogeneous graph neural network presented in Section IV. Unless specified otherwise, the BHGNN is trained for the setting of $N_t = 16, L = 4, M = 4$, and $K = 8$, and is tested with different settings to show its generalizability capability.
3) *Naive CNN*: Conventional CNN design that processes the entire channel matrices $\mathbf{H}$ and $\mathbf{G}$. We follow a similar architecture in [32] where the beamforming vector, STAR-RIS phase shift, and amplitude are jointly optimized

TABLE I
Parameters of the designed fully connected layer networks

Name	Shape	Activation function
f_{ϕ}^1, f_{ψ}^1	$2 + 2N_t \times 2 + 2N_t$	ReLU
f_{ϕ}^2, f_{ϕ}^3,f_{ψ}^2, f_{ψ}^3	574×574	ReLU
$f_{\mathcal{U}}^1$, $f_{\mathcal{B}}^1$	$2 + 2N_t \times 256$	ReLU
$f_{\mathcal{U}}^2$, $f_{\mathcal{B}}^2$,$f_{\mathcal{U}}^3$, $f_{\mathcal{B}}^3$	574×256	ReLU
$f_{\mathcal{W}}$	$256 \times 256 \times 2N_t$	ReLU
$f_{\mathcal{C}}$	$256 \times 64 \times 2$	Sigmoid
$f_{\mathcal{D}}$	$256 \times 64 \times 1$	Sigmoid

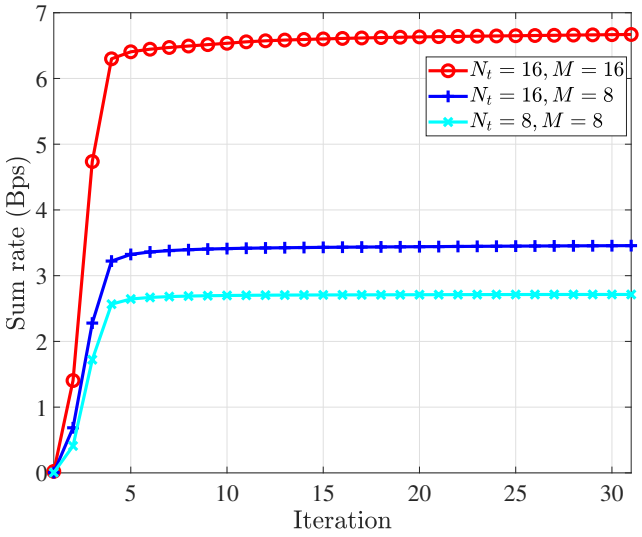

Fig. 3. The convergence behavior of the proposed AO-based algorithm with $K = 2, L = 4$.

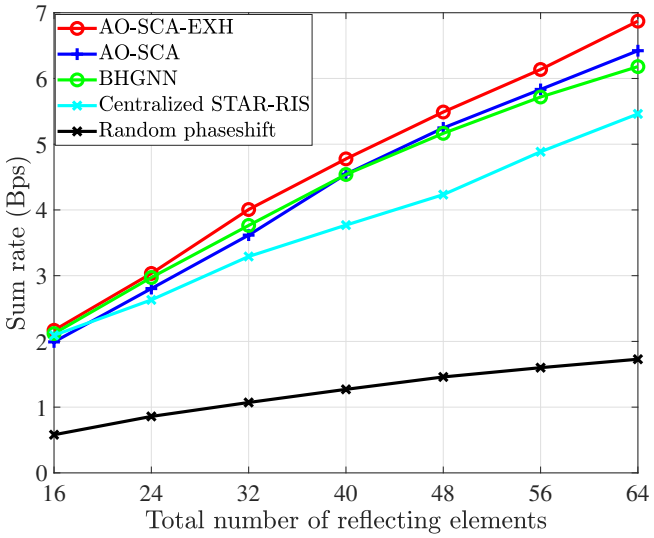

Fig. 4. The sum rate performance versus total number of scattering coefficients of the examined methods, with $K = 8, N_t = 16$.

4) *Centralized STAR-RIS*: We apply Algorithm 2 to optimize beamforming vectors, phase shift, and amplitude of the system with a single STAR-RIS located near the users.
5) *Random Phase shift*: We optimize beamforming vectors with the method proposed in Algorithm 2, while the phase shift and amplitude of the STAR-RISs are randomized.
6) AO-SCA-EXH: We run the proposed AO-SCA algorithm with different initialization points for a sufficiently large number and output the solution with the highest sum rate performance. Since Algorithm 2 is proved to converge to the KKT point, this scheme is expected to approximate the optimal solution wells.

B. Performance Evaluation

We first evaluate the convergence behavior of the proposed AO-based algorithm concerning the system sum rate. We present the system sum rate performance at each inner iteration of the AO-based algorithm with different settings. As depicted in Fig. 3, the AO algorithm demonstrates rapid convergence across all the examined configurations $(N_t, M) = (16, 16), (16, 8)$, and $(8, 8)$. Next, we compare the sum rate performance of the examined benchmarks versus the number of total scattering coefficients and illustrate the results in Fig. 4. In addition, to show the superiority of the distributed STAR-RIS system, we also present the performance of the single STAR-RIS-assisted system with an equal number of scattering elements. As can be observed, the random phase-shift benchmark still achieves a small gain, while the sum rate of the others examined frameworks grows significantly as the number of scattering elements grows. Particularly, the proposed AO algorithm and BHGNN yield a near-performance compared to the exhaustive scheme, i.e. the AO-SCA-EXH benchmark. As the number of scattering elements increases, the gap to an exhaustive search becomes larger. This is straightforward since in higher dimensions, the optimization

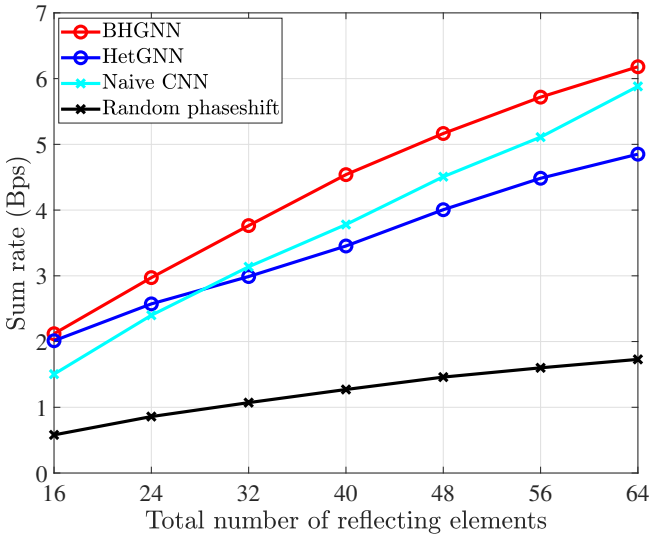

Fig. 5. The sum rate performance versus total number of scattering coefficients of different ML-based methods, with $K = 8, N_t = 16$.

space is extremely large. The algorithm is, therefore, more likely to converge to a local optimal solution. While the BHGNN is trained with $(L, M) = (4, 8)$, it generalizes well with different numbers of scattering coefficients.

Next, we compare the proposed BHGNN model with other existing deep learning designs in Fig. 5. The HetGNN scheme denotes a heterogeneous graph neural network design with the vertices and edges defined similarly to the proposed BHGNN. However, we adopt the conventional message passing procedure in [20] to optimize this scheme. As shown in Fig. 5, the proposed BHGNN outperforms other DL models. Although the Naive CNN model can achieve a close performance compared to BHGNN, it is required to be re-trained for different numbers of reflecting coefficients. In addition, the performance of the HetGNN model is notably inferior to that of the the

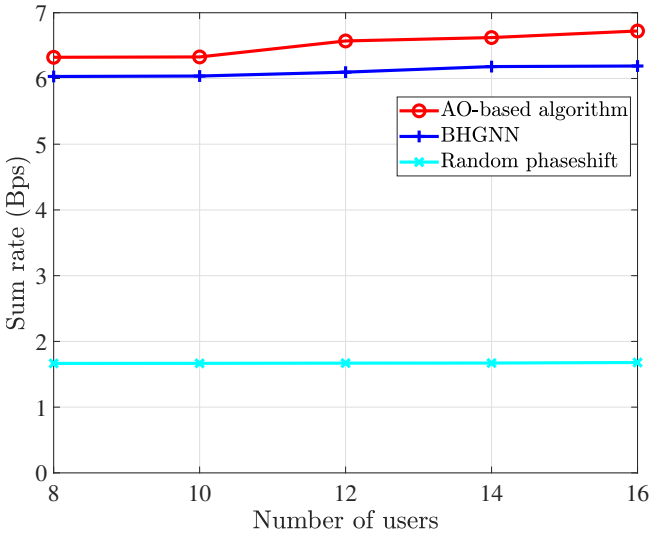

Fig. 6. The sum rate performance versus number of users with $N_t = 16$, $L = 4$, $M = 16$.

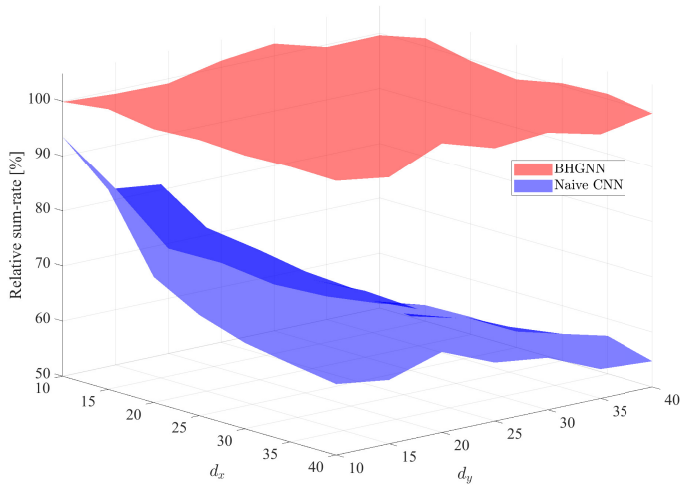

Fig. 7. The sum rate performance versus different user location's density, with $N_t = 16$, $L = 4$, $M = 10$, $K = 8$.

proposed BHGNN which validates the effectiveness of our proposed message-passing inference. Furthermore, as shown in Fig. 6, the proposed BHGNN generalizes well with different numbers of users with comparable performance to the AO-based algorithm. This is crucial since unlike the conventional DNN models, the proposed BHGNN does not require to be re-trained when the system settings are changed.

In Fig. 7, we illustrate the relative sum rate performance yielded by the proposed HGNN and naive CNN model as a function of different user location densities. The relative sum rate is defined as the sum rate normalized by that of the AO-SCA algorithm. Specifically, the DL models are first trained as users are uniformly distributed in the rectangular area of $(x, y) = [\pm 20, \pm 30] \times [20, 30]$. We then vary the area of the rectangle in the testing phase as $(x, y) = [20, 20 + d_x] \times [20, 20 + d_y]$ for T users and $(x, y) = [-20 - d_x, -20] \times [20, 20 + d_y]$ for R users, where d_x and d_y denote the range of the location rectangle. Even though most of the user locations are unseen in the testing phase, the design HGNN obtains almost a similar sum rate compared to the AO-SCA algorithm. In contrast, naive CNN yields significant performance losses, particularly when the network area is larger. This validates the scalability to different user locations of our proposed HGNN model. Unlike the naive CNN model which simply memorizes the mapping between channel information and the optimal solution, the HGNN model learns the universal optimization rule which allows it to generalize well to different system configurations.

VI. Conclusion

In this paper, we idelved into the joint optimization of active and passive beamforming in a distributed STAR-RIS assisted MU-MISO communication networks to maximize the overall sum rate. We proposed two novel approaches that efficiently handle the inherent non-convexity of the original problem. First, we designed an alternating algorithm based on the SCA method with a provable convergence to iteratively solve the original problem with subject to transmit beamforming vectors, STAR-RIS phase shifts, and STAR-RIS amplitude coefficients. Furthermore, we proposed a HGNN design to directly optimize the beamforming vectors and STAR-RIS scattering coefficients, namely BHGNN. Particularly, we modeled each user and STAR-RIS coefficient as vertices, while the effective channel information was exploited as edges connecting them. Numerical results showed that the proposed BHGNN model can achieve a comparable sum rate performance to the iterative one, and it can generalize well with different number of users as well as STAR-RIS coefficients.

Appendix A
Proof of Lemma 1

For simplicity, we rewrite the original problem (5) as

$$\underset{\mathbf{x}}{\text{minimize}} \quad f_0(\mathbf{x}) \tag{43a}$$

$$\text{subject to} \quad f_i(\mathbf{x}) \leq 0, \quad i = 1, \ldots, m \tag{43b}$$

where $f_0(\mathbf{x})$ is the negative original objective function, $f_i(\mathbf{x}), i = 1, \ldots, m-1$ are differentiable convex functions, $f_m(\mathbf{x})$ is a differentiable function, i.e. the constraint (14). The non-convex problem is solved by using SCA procedure with approximated optimization problem defined as

$$\underset{\mathbf{x}}{\text{minimize}} \quad \bar{f}_0(\mathbf{x}, \mathbf{x}^{(n)}) \tag{44a}$$

$$\text{subject to} \quad f_i(\mathbf{x}) \leq 0, \quad i = 1, \ldots, m-1, \tag{44b}$$

$$\bar{f}_m(\mathbf{x}, \mathbf{x}^n) \leq 0. \tag{44c}$$

We first start by giving a lemma that is essential for the proof.

Lemma 2. *If the step-size $\gamma^{(n)}$ is chosen according to the diminishing rule, then*

$$\lim_{n \to \infty} ||\mathbf{x}^{(n)} - \hat{\mathbf{x}}^{(n)}|| = 0, \tag{45}$$

where $\hat{\mathbf{x}}^{(n)}$ is the optimal solution for problem (44).

Proof: It follows from (52) *and* $\sum_{n=1}^{\infty}\gamma^{(n)}=\infty$ *that* $\liminf_{n\to\infty}||\mathbf{x}^{(n)}-\hat{\mathbf{x}}^{(n)}||=0$. *To prove* $\limsup_{t\to\infty}||\mathbf{x}^{(n)}-\hat{\mathbf{x}}^{(n)}||=0$, *we follow the contradiction proof in appendix B in [33]. Finally, the iterative algorithm guarantees that* $\mathbf{x}^{(n)}$ *will finally converge to* $\hat{\mathbf{x}}^{(n)}$. ∎

Lemma 2 states that when the step-size is properly chosen, the gap between $\mathbf{x}^{(n)}$ and $\hat{\mathbf{x}}^{(n)}$ will converge to zero. We then prove that the approximated problem (44) will converge to the feasible region of the original problem (5). Since $\bar{f}_m(\mathbf{x},\mathbf{x}^{(n)})$ is convex, we have

$$\bar{f}_m(\hat{\mathbf{x}}^{(n)},\mathbf{x}^{(n)})-\bar{f}_m(\mathbf{x}^{(n)},\mathbf{x}^{(n)})\geq\nabla\bar{f}_m(\mathbf{x}^{(n)},\mathbf{x}^{(n)})(\hat{\mathbf{x}}^{(n)}-\mathbf{x}^{(n)})+\eta||\hat{\mathbf{x}}^{(n)}-\mathbf{x}^{(n)}||^2, \tag{46}$$

where $\eta>0$ is some constant. Moreover, it is easy to see that derivative of $f_m(\mathbf{x})$ is Lipschitz continuous, thus the Descent Lemma [34] yield

$$\begin{aligned}
&f_m(\mathbf{x}^{(n+1)})\leq f_m(\mathbf{x}^{(n)})+\gamma^{(n)}\nabla f_m(\mathbf{x}^{(n)})\mathbf{d}^{(n)}\\
&+L_f(\gamma^{(n)})^2||\mathbf{d}^{(n)}||^2\\
&=f_m(\mathbf{x}^{(n)})+L_f(\gamma^{(n)})^2||\mathbf{d}^{(n)}||^2\\
&+\gamma^{(n)}\nabla\bar{f}_m(\mathbf{x}^{(n)},\mathbf{x}^{(n)})\mathbf{d}^{(n)}\\
&\leq f_m(\mathbf{x}^{(n)})+L_f(\gamma^{(n)})^2||\mathbf{d}^{(n)}||^2-\gamma^{(n)}\eta||\mathbf{d}^{(n)}||^2\\
&+\gamma^{(n)}(\bar{f}_m(\hat{\mathbf{x}}^{(n)},\mathbf{x}^{(n)})-\bar{f}_m(\mathbf{x}^{(n)},\mathbf{x}^{(n)}))\\
&\leq f_m(\mathbf{x}^{(n)})-\gamma^{(n)}\eta||\mathbf{d}^{(n)}||^2+L_f(\gamma^{(n)})^2||\mathbf{d}^{(n)}||^2\\
&+\gamma^{(n)}||\bar{f}_m(\hat{\mathbf{x}}^{(n)},\mathbf{x}^{(n)})-\bar{f}_m(\mathbf{x}^{(n)},\mathbf{x}^{(n)})||\\
&\leq f_m(\mathbf{x}^{(n)})-\gamma^{(n)}\eta||\mathbf{d}^{(n)}||^2+\gamma^{(n)}B||\mathbf{d}||+o\left(\gamma^{(n)}\right),
\end{aligned} \tag{47}$$

where $\mathbf{d}^{(n)}=\hat{\mathbf{x}}^{(n)}-\mathbf{x}^{(n)}$, $L_f>0,\eta>0,B>0$ are any constants, and $o\left(\gamma^{(n)}\right)$ means $\lim_{n\to\infty}o\left(\gamma^{(n)}\right)/\gamma^{(n)}=0$. By choosing a sufficiently large t_ϵ and applying Lemma 2, we have

$$f_m(\mathbf{x}^{(n+1)})-f_m(\mathbf{x}^{(n)})\leq 0. \tag{48}$$

Furthermore, since $f_m(\mathbf{x})$ is Lipschitz continuous, we have

$$|f_m(\mathbf{x}^{(n+1)})-f_m(\mathbf{x}^{(n)})|\leq O(||\mathbf{x}^{(n+1)}-\mathbf{x}^{(n)}||)\leq O(\gamma^{(n)})\leq\epsilon, \tag{49}$$

with $\forall n\geq n_\epsilon$, where the last inequality is due to $\gamma^n\to 0$ as $n\to\infty$. From (48), we can see that $f_m(\mathbf{x}^{(n)})$ is decreased when $f_m(\mathbf{x}^{(n)})>\epsilon$ and $n\geq n_\epsilon$. Therefore, from (48) and (49), we have

$$f_m(\mathbf{x}^{(n)})\leq 2\epsilon,\forall n\geq n_\epsilon. \tag{50}$$

Since the inequalities hold for any $\epsilon>0$, it follows that $\limsup_{n\to\infty}f_m(\mathbf{x}^{(n)})\leq 0$. Therefore, the problem (44) is guaranteed to be converged to the feasible region of problem (43).

Next, we prove the convergence of the original problem (43). Following the similar topology in appendix B of [33] and the descent lemma, it can be shown that

$$f_0(\mathbf{x}^{(n+1)})\leq f_0(\mathbf{x}^{(n)})-\gamma^{(n)}\beta_1||\bar{\mathbf{x}}^{(n)}-\mathbf{x}^{(n)}||^2, \tag{51}$$

where $\beta_1>0$ is a constant. By invoking Lemma 7 in [33] with $X^t=f_0(\mathbf{x}^{(n+1)})$, $Y^t=\gamma^{(n)}\beta_1||\bar{\mathbf{x}}^{(n)}-\mathbf{x}^{(n)}||^2$, and $Z^t=0$, we can conclude from (51) that either $\{f_0(\mathbf{x}^{(n)})\}\to-\infty$ or it converges to a finite value and

$$\lim_{n\to\infty}\sum_n\gamma^n||\bar{\mathbf{x}}^{(n)}-\mathbf{x}^{(n)}||^2<+\infty. \tag{52}$$

Obviously, $f_0(\mathbf{x})$ is bounded due to the power constraint and unit-modulo constraint, thus it is convergent. Finally, by denoting $\mathbf{x}^*$ the limit point of the sequence $\{\mathbf{x}^{(n)}\}$, from lemma 2, we have $\mathbf{x}^*=\hat{\mathbf{x}}^\infty$. Since $\mathbf{x}^*$ is a solution for the convex problem (44), it is a KKT point. Therefore,

$$\begin{aligned}
&\nabla f_0(\mathbf{x}^*)+\sum_{i=1}^{l}\lambda_i\nabla f_i(\mathbf{x}^*)+\lambda_m\nabla\bar{f}_m(\mathbf{x}^*,\mathbf{x}^*)=0\\
&\lambda_i f_i(\mathbf{x}^*)=0,i=1,\ldots,m-1;\quad\lambda_m\bar{f}_m(\mathbf{x}^*,\mathbf{x}^*)=0,
\end{aligned} \tag{53}$$

where λ_i is the dual variable associated with the i-th constraint. By replacing $\bar{f}_m(\mathbf{x}^*,\mathbf{x}^*)$ with $f_m(\mathbf{x}^*)$ and $\nabla\bar{f}_m(\mathbf{x}^*,\mathbf{x}^*)$ with $\nabla f_m(\mathbf{x}^*)$, we have

$$\begin{aligned}
&\nabla f_0(\mathbf{x}^*)+\sum_{i=1}^{l}\lambda_i\nabla f_i(\mathbf{x}^*)=0\\
&\lambda_i f_i(\mathbf{x}^*)=0,i=1,\ldots,m.
\end{aligned} \tag{54}$$

Therefore, $\mathbf{x}^*$ is also the KKT solution for problem (43).

Appendix B
Proof of Proposition 2

We denote the input feature of user vertex k and RIS vertex r in the original graph as $\mathbf{u}_k^{(0)}$ and $\mathbf{b}_r^{(0)}$, the edge feature connecting RIS vertex r and user vertex k as $\mathbf{e}_{r,k}$, and the output of the t-th layer as $\mathbf{u}_k^{(t)}$ and $\mathbf{b}_r^{(t)}$. These variables in the permuted graph are correspondingly denoted as $\hat{\mathbf{u}}_k^{(0)}$, $\hat{\mathbf{b}}_r^{(0)}$, $\hat{\mathbf{e}}_{r,k}$, $\hat{\mathbf{u}}_k^{(t)}$, and $\hat{\mathbf{b}}_r^{(t)}$. At the initial stage of the graph, we have

$$\begin{aligned}
&\hat{\mathbf{e}}_{\pi_1(r),\pi_2(k)}=\mathbf{e}_{r,k},\quad\hat{\mathbf{b}}_{\pi_1(r)}^{(0)}=\mathbf{b}_r^{(0)},\quad\hat{\mathbf{u}}_{\pi_2(k)}^{(0)}=\mathbf{u}_k^{(0)},\\
&\mathcal{R}(\pi_1(r))=\{\pi_1(r),r\in\mathcal{R}\},\quad\mathcal{K}(\pi_2(k))=\{\pi_2(k),k\in\mathcal{K}\},
\end{aligned} \tag{55}$$

where π_1 and π_2 are the permutation operator on the RIS vertices and user vertices. Specifically, these operators are defined as

$$\begin{aligned}
\pi_1:[LM]\to[LM]\quad\text{with}\quad[LM]=\{1,\ldots LM\}\\
\pi_2:[K]\to[K]\quad\text{with}\quad[K]=\{1,\ldots,K\}
\end{aligned} \tag{56}$$

For given permutation operators π_1, π_2 and n, we prove that $\mathbf{u}_k^{(n)}=\hat{\mathbf{u}}_{\pi_2(k)}^{(n)},\forall k$, and $\mathbf{b}_r^{(n)}=\hat{\mathbf{b}}_{\pi_1(r)}^{(n)},\forall n$ by induction. In the case of $n=0$, the proof follows directly (55). We now assume that the result holds with $n=1,\ldots,s-1$, that is

$$\begin{aligned}
&\mathbf{u}_k^{(n)}=\hat{\mathbf{u}}_{\pi_2(k)}^{(n)},\quad\mathbf{b}_r^{(n)}=\hat{\mathbf{b}}_{\pi_1(r)}^{(n)},\hat{\mathbf{e}}_{\pi_1(r),\pi_2(k)}=\mathbf{e}_{r,k},\\
&\mathcal{R}(\pi_1(r))=\{\pi_1(r),r\in\mathcal{R}\},\quad\mathcal{K}(\pi_2(k))=\{\pi_2(k),k\in\mathcal{K}\},\\
&\forall n=1,\ldots,s-1.
\end{aligned} \tag{57}$$

We prove that the results hold with $n=s$. Following the GMP update rule, the outputs of vertices at the s-th layer are

$$\mathbf{u}_k^{(s)}=\mathcal{U}^s\left(\mathbf{u}_k^{(s-1)},\mathcal{W}(\mathbf{u}_k^{(s-1)}),\right.$$

$$\mathrm{PL}_{r\in\mathcal{R}}\left\{\phi^s(\mathbf{b}_r^{(s-1)},\mathbf{u}_k^{(s-1)},\mathbf{e}_{r,k})\right\}\Big),$$
$$\hat{\mathbf{u}}^s_{\pi_2(k)}=\mathcal{U}^s\Big(\mathbf{u}^{(s-1)}_{\pi_2(k)},\mathcal{W}(\mathbf{u}^{(s-1)}_{\pi_2(k)}),$$
$$\mathrm{PL}_{r\in\mathcal{R}(\pi_1(r))}\left\{\phi^s(\mathbf{b}_r^{(s-1)},\mathbf{u}^{(s-1)}_{\pi_2(k)},\mathbf{e}_{r,\pi_2(k)})\right\}\Big),$$
$$\mathbf{b}_r^{(s)}=\mathcal{B}^s\Big(\mathbf{b}_r^{(s-1)},\mathcal{C}(\mathbf{b}_r^{(s-1)}),\mathcal{D}(\mathbf{b}_r^{(s-1)}),$$
$$\mathrm{PL}_{k\in\mathcal{K}}\left\{\psi^s(\mathbf{u}_k^{(s-1)},\mathbf{b}_r^{(s-1)},\mathbf{e}_{r,k})\right\}\Big)$$
$$\hat{\mathbf{b}}^{(s)}_{\pi_1(r)}=\mathcal{B}^s\Big(\mathbf{b}^{(s-1)}_{\pi_1(r)},\mathcal{C}(\mathbf{b}^{(s-1)}_{\pi_1(r)}),\mathcal{D}(\mathbf{b}^{(s-1)}_{\pi_1(r)}),$$
$$\mathrm{PL}_{k\in\mathcal{K}(\pi_2(k))}\left\{\psi^s(\mathbf{u}_k^{(s-1)},\mathbf{b}^{(s-1)}_{\pi_1(r)},\mathbf{e}_{\pi_1(r),k})\right\}\Big). \quad (58)$$

Plugging (57) into (58), we have $\mathbf{u}_k^{(s)}=\hat{\mathbf{u}}^{(s)}_{\pi(k)}$ and $\mathbf{b}_r^{(s)}=\hat{\mathbf{b}}^{(s)}_{\pi(r)}$. We recall that for the original graph, the output at RIS vertices is $\mathbf{U}=[\mathbf{u}_1,\ldots,\mathbf{u}_{|\mathcal{R}|}]^T$, while that of the permuted graph is $\hat{\mathbf{U}}=[\hat{\mathbf{u}}_1,\ldots,\hat{\mathbf{u}}_{|\mathcal{R}|}]^T$. Therefore, we have $\mathbf{U}=\pi_1\star\hat{\mathbf{U}}$. Similarly, we have $\mathbf{B}=\pi_2\star\hat{\mathbf{B}}$, where $(\pi_1\star\hat{\mathbf{U}})_{\pi_1(r)}=\mathbf{U}_r$. Since permutation of the output of the original graph is the output of the permuted graph, the result in proposition 2 is proved.

REFERENCES

[1] W. Saad, M. Bennis, and M. Chen, "A vision of 6g wireless systems: Applications, trends, technologies, and open research problems," *IEEE Network*, vol. 34, no. 3, pp. 134–142, 2020.

[2] E. Basar, M. Di Renzo, J. De Rosny, M. Debbah, M.-S. Alouini, and R. Zhang, "Wireless communications through reconfigurable intelligent surfaces," *IEEE Access*, vol. 7, pp. 116 753–116 773, 2019.

[3] X. Mu, Y. Liu, L. Guo, J. Lin, and R. Schober, "Simultaneously transmitting and reflecting (star) ris aided wireless communications," *IEEE Transactions on Wireless Communications*, vol. 21, no. 5, pp. 3083–3098, 2022.

[4] T. Wang, F. Fang, and Z. Ding, "Joint phase shift and beamforming design in a multi-user miso star-ris assisted downlink noma network," *IEEE Transactions on Vehicular Technology*, vol. 72, no. 7, pp. 9031–9043, 2023.

[5] C. Wu, Y. Liu, X. Mu, X. Gu, and O. A. Dobre, "Coverage characterization of star-ris networks: Noma and oma," *IEEE Communications Letters*, vol. 25, no. 9, pp. 3036–3040, 2021.

[6] A. Papazafeiropoulos, C. Pan, A. Elbir, P. Kourtessis, S. Chatzinotas, and J. M. Senior, "Coverage probability of distributed irs systems under spatially correlated channels," *IEEE Wireless Communications Letters*, vol. 10, no. 8, pp. 1722–1726, 2021.

[7] P. Wang, J. Fang, X. Yuan, Z. Chen, and H. Li, "Intelligent reflecting surface-assisted millimeter wave communications: Joint active and passive precoding design," *IEEE Transactions on Vehicular Technology*, vol. 69, no. 12, pp. 14 960–14 973, 2020.

[8] Z. Yang, M. Chen, W. Saad, W. Xu, M. Shikh-Bahaei, H. V. Poor, and S. Cui, "Energy-efficient wireless communications with distributed reconfigurable intelligent surfaces," *IEEE Transactions on Wireless Communications*, vol. 21, no. 1, pp. 665–679, 2022.

[9] H. Sun, X. Chen, Q. Shi, M. Hong, X. Fu, and N. D. Sidiropoulos, "Learning to optimize: Training deep neural networks for interference management," *IEEE Transactions on Signal Processing*, vol. 66, no. 20, pp. 5438–5453, 2018.

[10] H. Huang, Y. Song, G. Gui, and F. Adachi, "Deep-learning-based millimeter-wave massive MIMO for hybrid precoding," *IEEE Transactions on Vehicular Technology*, vol. 68, no. 3, pp. 3027–3032, 2019.

[11] X. Li and A. Alkhateeb, "Deep learning for direct hybrid precoding in millimeter wave massive MIMO systems," in *2019 53rd Asilomar Conference on Signals, Systems, and Computers*, 2019, pp. 800–805.

[12] W. Xu, L. Gan, and C. Huang, "A robust deep learning-based beamforming design for RIS-assisted multiuser MISO communications with practical constraints," *IEEE Transactions on Cognitive Communications and Networking*, vol. 8, no. 2, pp. 694–706, 2022.

[13] H. An Le, T. Van Chien, V. D. Nguyen, and W. Choi, "Double ris-assisted mimo systems over spatially correlated rician fading channels and finite scatterers," *IEEE Transactions on Communications*, vol. 71, no. 8, pp. 4941–4956, 2023.

[14] Y. Guo, F. Fang, D. Cai, and Z. Ding, "Energy-efficient design for a noma assisted star-ris network with deep reinforcement learning," *IEEE Transactions on Vehicular Technology*, vol. 72, no. 4, pp. 5424–5428, 2023.

[15] J. Zhou, G. Cui, S. Hu, Z. Zhang, C. Yang, Z. Liu, L. Wang, C. Li, and M. Sun, "Graph neural networks: A review of methods and applications," *AI Open*, vol. 1, pp. 57–81, 2020.

[16] Y. Shen, J. Zhang, S. H. Song, and K. B. Letaief, "Graph neural networks for wireless communications: From theory to practice," *IEEE Transactions on Wireless Communications*, vol. 22, no. 5, pp. 3554–3569, 2023.

[17] M. Eisen and A. Ribeiro, "Optimal wireless resource allocation with random edge graph neural networks," *IEEE Transactions on Signal Processing*, vol. 68, pp. 2977–2991, 2020.

[18] Y. Shen, Y. Shi, J. Zhang, and K. B. Letaief, "Graph neural networks for scalable radio resource management: Architecture design and theoretical analysis," *IEEE Journal on Selected Areas in Communications*, vol. 39, no. 1, pp. 101–115, 2021.

[19] A. Chowdhury, G. Verma, C. Rao, A. Swami, and S. Segarra, "Unfolding wmmse using graph neural networks for efficient power allocation," *IEEE Transactions on Wireless Communications*, vol. 20, no. 9, pp. 6004–6017, 2021.

[20] J. Guo and C. Yang, "Learning power allocation for multi-cell-multi-user systems with heterogeneous graph neural networks," *IEEE Transactions on Wireless Communications*, vol. 21, no. 2, pp. 884–897, 2022.

[21] J. Kim, H. Lee, S.-E. Hong, and S.-H. Park, "A bipartite graph neural network approach for scalable beamforming optimization," *IEEE Transactions on Wireless Communications*, vol. 22, no. 1, pp. 333–347, 2023.

[22] T. Jiang, H. V. Cheng, and W. Yu, "Learning to reflect and to beamform for intelligent reflecting surface with implicit channel estimation," *IEEE Journal on Selected Areas in Communications*, vol. 39, no. 7, pp. 1931–1945, 2021.

[23] Z.-Q. Luo and S. Zhang, "Dynamic spectrum management: Complexity and duality," *IEEE journal of selected topics in signal processing*, vol. 2, no. 1, pp. 57–73, 2008.

[24] M. S. Lobo, L. Vandenberghe, S. Boyd, and H. Lebret, "Applications of second-order cone programming," *Linear Algebra and its Applications*, vol. 284, no. 1, pp. 193–228, 1998.

[25] X. Zhang, H. Zhao, J. Xiong, X. Liu, L. Zhou, and J. Wei, "Scalable power control/beamforming in heterogeneous wireless networks with graph neural networks," in *2021 IEEE Global Communications Conference (GLOBECOM)*, 2021, pp. 01–06.

[26] K. Hornik, M. Stinchcombe, and H. White, "Multilayer feedforward networks are universal approximators," *Neural Networks*, vol. 2, no. 5, pp. 359–366, 1989.

[27] D. P. Kingma and J. Ba, "Adam: A method for stochastic optimization," in *3rd International Conference on Learning Representations, ICLR 2015, San Diego, CA, USA, May 7-9, 2015, Conference Track Proceedings*, Y. Bengio and Y. LeCun, Eds., 2015.

[28] H. A. Le, T. Van Chien, T. H. Nguyen, H. Choo, and V. D. Nguyen, "Machine learning-based 5g-and-beyond channel estimation for mimo-ofdm communication systems," *Sensors*, vol. 21, no. 14, 2021.

[29] S. Zhang and R. Zhang, "Capacity characterization for intelligent reflecting surface aided MIMO communication," *IEEE Journal on Selected Areas in Communications*, vol. 38, no. 8, pp. 1823–1838, 2020.

[30] A. Paszke, S. Gross, F. Massa, A. Lerer, J. Bradbury *et al.*, "Pytorch: An imperative style, high-performance deep learning library," in *Advances in Neural Information Processing Systems 32*. Curran Associates, Inc., 2019, pp. 8024–8035.

[31] K. Diederik P and B. Jimmy, "Adam: A method for stochastic optimization," 2014, available: https://arxiv.org/abs/1412.6980.

[32] H. Song, M. Zhang, J. Gao, and C. Zhong, "Unsupervised learning-based joint active and passive beamforming design for reconfigurable intelligent surfaces aided wireless networks," *IEEE Communications Letters*, vol. 25, no. 3, pp. 892–896, 2021.

[33] G. Scutari, F. Facchinei, P. Song, D. P. Palomar, and J.-S. Pang, "Decomposition by partial linearization: Parallel optimization of multi-agent systems," *IEEE Transactions on Signal Processing*, vol. 62, no. 3, pp. 641–656, 2014.

[34] D. P. Bertsekas, "Nonlinear programming," *Journal of the Operational Research Society*, vol. 48, no. 3, pp. 334–334, 1997.